In-band Spectrum Sensing in Cognitive Radio Networks: Energy Detection or Feature Detection?

Hyoil Kim and Kang G. Shin
Real-Time Computing Laboratory, EECS Department
The University of Michigan, Ann Arbor, MI 48109-2121, USA.
{hyoilkim, kgshin}@eecs.umich.edu

ABSTRACT

In a cognitive radio network (CRN), in-band spectrum sensing is essential for the protection of legacy spectrum users, with which the presence of primary users (PUs) can be detected promptly, allowing secondary users (SUs) to vacate the channels immediately. For in-band sensing, it is important to meet the detectability requirements, such as the maximum allowed latency of detection (e.g., 2 seconds in IEEE 802.22) and the probability of mis-detection and false-alarm. In this paper, we propose an efficient periodic in-band sensing algorithm that optimizes sensing-frequency and sensing-time by minimizing sensing overhead while meeting the detectability requirements. The proposed scheme determines the better of energy or feature detection that incurs less sensing overhead at each SNR level, and derives the threshold $aRSS_{threshold}$ on the average received signal strength (RSS) of a primary signal below which feature detection is preferred. We showed that energy detection under lognormal shadowing could still perform well at the average SNR $< SNR_{wall}$ [1] when collaborative sensing is used for its location diversity. Two key factors affecting detection performance are also considered: noise uncertainty and inter-CRN interference. $aRSS_{threshold}$ appears to lie between -114.6 dBm and -109.9 dBm with the noise uncertainty ranging from 0.5 dB to 2 dB, and between -112.9 dBm and -110.5 dBm with 1$\sim$6 interfering CRNs.

Categories and Subject Descriptors

C.2.1 [**Computer-Communication Networks**]: Network Architecture and Design— *Wireless communication*

General Terms

Algorithms, Design, Performance, Theory

Keywords

Spectrum sensing and opportunity, sensor clustering, sensing scheduling, energy and feature detection

MobiCom'08, September 14–19, 2008, San Francisco, California, USA.

1. INTRODUCTION

Cognitive radio (CR) is a key technology for alleviating the inefficient spectrum-utilization problem under the current static spectrum-allocation policy [2–4]. In cognitive networks (CRNs), unlicensed or secondary users (SUs) are allowed to opportunistically utilize spectrum bands assigned to licensed or primary users (PUs) as long as they do not cause any harmful interference to PUs. A *spectrum opportunity* refers to a time duration on a channel[1] during which the channel can be used by SUs without interfering with the channel's PUs. *In-band* channels refer to those channels currently in use by SUs; all others are referred to as *out-of-band* channels.

One of the major challenges in CRNs is to strike a balance between (1) protection of PUs against interference from SUs and (2) efficient reuse of legacy spectrum, for which *spectrum sensing* is essential. That is, spectrum sensing discovers spectrum opportunities or holes by monitoring out-of-band channels and detecting white spaces [5]. When thus-discovered opportunities are utilized by SUs, in-band spectrum sensing must promptly detect return of PUs to an in-band channel so that SUs can vacate the channel immediately upon detection of returning PUs.

For maximal protection of PUs, FCC has set a strict guideline on in-band sensing. For example, in IEEE 802.22, the world's first international CR standard,[2] PUs should be detected within 2 seconds of their appearance with the probability of misdetection (P_{MD}) and the probability of false detection (P_{FA}) less than 0.1. To meet these requirements, in-band sensing must be run frequently enough (at least once every 2 seconds) and a detection method (e.g., energy and feature detection [6]) that yields the best performance should be selected. Both the sensing frequency and the detection method should be chosen by considering the impact on SUs' QoS impairment since sensing should be performed during quiet periods [6, 7], i.e., communications between SUs are suspended.

This paper presents an efficient in-band sensing algorithm that (1) derives the period of sensing by minimizing the amount of sensing time, or *sensing overhead*, while meeting the detectability requirement, and (2) selects the detection method that incurs less sensing overhead. In what follows, we first advocate use of clustered sensor networks to support in-band spectrum sensing, identifying two im-

[1] *Spectrum band* and *channel* will be used interchangeably in this paper.
[2] Note that IEEE 802.22 is still a draft at the time of this writing.

portant research challenges. Second, we show how appropriate scheduling of in-band sensing can enhance the sensing performance and help support QoS in CRNs. We also show that SNR_{wall} [1] of energy detection, which acts as an absolute barrier in an AWGN channel, is breakable in a shadow-fading channel when the average SNR of collaborative sensors is less than SNR_{wall}. Based on this finding, energy detection is preferred to feature detection even at a very small SNR.

1.1 Sensor Clustering

1.1.1 Motivation

Collaborative sensing [8–10] is known to be essential for better detectability as it exploits sensor diversity via simultaneous sensing on a channel at multiple locations. Presence of PUs on a channel is determined by processing the measurements via data fusion. A common data fusion rule is the OR-rule [11] where PUs are considered present if at least one sensor reports their presence. Its sensing performance with N cooperative sensors has been shown as

$$P_{MD}(N) = {P_{MD}}^N, \text{ and } P_{FA}(N) = 1 - (1 - P_{FA})^N, \quad (1)$$

under the assumption that every sensor has the same P_{MD} and P_{FA} for a given signal.

Eq. (1), however, does not hold in a large CRN such as an IEEE 802.22 network in which a base station (BS) covers an area of radius ranging from 33 km (typical) to 100 km [6]. In such a case, the average received signal strength (RSS)[3] of a primary signal at two distant sensor locations (CPE A and CPE B in Fig. 1) may vary significantly. Heterogeneous P_{MD} and P_{FA} of each sensor must therefore be considered in modeling collaborative sensing performance, making it harder to design a collaborative sensor network (e.g., determining the number of cooperative sensors needed).

Sensor clustering avoids this problem by grouping sensors in close proximity into a cluster so that they can measure a similar average RSS of any primary signal. Sensor clustering also mitigates the control overhead in data fusion. Instead of forcing all sensors to report their measurements to the BS, each cluster head (CH) can collect intra-cluster measurements and make a local decision, which is then reported to the BS.

1.1.2 Contributions

Although there has been considerable research into clustered CR sensor networks [13–15], two important issues have not yet been addressed: (1) cluster size and (2) sensor density. Section 3 addresses these two issues as follows. First, we will derive the maximum radius of a cluster so as to upper-bound the variation of the average RSS in a cluster by 1 dB. Second, we will derive the maximum sensor density to guarantee near-independent sensor observations. Mishra *et al.* [16] claimed that 10–20 independent sensors perform better than many more correlated sensors since correlation between sensors due to shadow fading limits the collaborative sensing gain. Since the correlation between two sensors decreases exponentially as distance between sensors grows linearly [17], we can upper-bound sensor density such that the average distance between neighboring sensors is lower-bounded and the shadow correlation is smaller than 0.3.

With this approach, one-time (collaborative) in-band sensing in a cluster can be completely described by Eq. (1) where N now becomes the number of cooperative sensors within a cluster. Next, we consider periodic scheduling of in-band sensing and its related issues.

1.2 Scheduling of In-band Sensing

1.2.1 Motivation

IEEE 802.22 requires in-band sensing to achieve $P_{MD} \leq 0.1$ in detecting the presence of primary signals within a channel detection latency threshold CDT which is typically 2 seconds. P_{FA} is interpreted similarly: $P_{FA} \leq 0.1$ should be achieved if the sensing algorithm runs for CDT seconds when no PUs are present.

IEEE 802.22 also provides the *two-stage sensing* (TSS) mechanism where a sensing algorithm can decide which of energy or feature detection is used in a quiet period. Although energy detection incurs minimal time overhead (usually less than 1 ms), its susceptibility to noise uncertainty [1] limits its usability. Feature detection is less susceptible to noise uncertainty [18] but it requires a longer sensing time (e.g., 24.2 ms for the field sync detector [6]).

The current IEEE 802.22 draft does not specify how often sensing must be scheduled and which detection method to use, and under what condition. Although there have been several studies on the performance of energy and feature detection [6, 19–23], they were all based on one-time detection. Hence, we propose an efficient sensing algorithm that (1) minimizes sensing overhead by optimizing the sensing period (T_P in Fig. 2) and the sensing time (T_I in Fig. 2), and (2) chooses the better of energy or feature detection in a given sensing environment.

1.2.2 Contributions

SNR_{wall} [1] implies the minimum SNR threshold due to noise uncertainty below which a detector cannot reliably identify a primary signal, regardless of how much time it takes. SNR_{wall} of energy detection is often understood as an absolute barrier, and hence, energy detection completely fails at a very low SNR. However, we will show that SNR_{wall} is an absolute barrier only in the AWGN channel, and in reality, the barrier becomes obscure with the shadowing channel. As a result, in most cases energy detection is still a good candidate for sensing because of its low sensing-time. That is, although feature detection may perform better than energy detection with one-time sensing, energy detection can outperform feature detection by sensing more frequently.

Two important factors affecting the detection performance—noise uncertainty and inter-CRN interference—will also be investigated and their effects will be evaluated extensively. We will finally propose a sensing strategy to decide the best detection method for a given sensing condition.

1.3 Related Work

There have been continuing discussions on using clustered networks in CRs. Chen *et al.* [13] proposed a mechanism to form a cluster among neighboring nodes and then interconnect such clusters. Pawelczak *et al.* [15] proposed cluster-based sensor networks to reduce the latency in reporting sensor measurements by designating the cluster head as a

[3]Note that the "average" received singal strength (aRSS) is the *empirical* large-scale path loss of the shadow fading model introduced in [12].

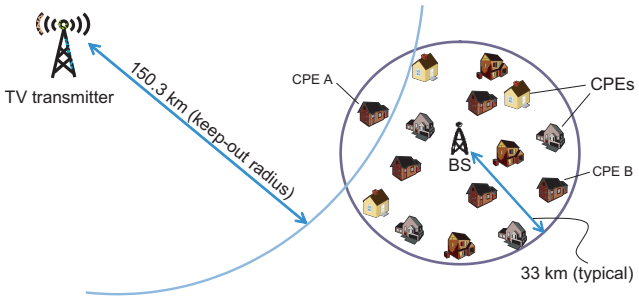

Figure 1: Illustration of an IEEE 802.22 cell which coexists with a TV transmitter.

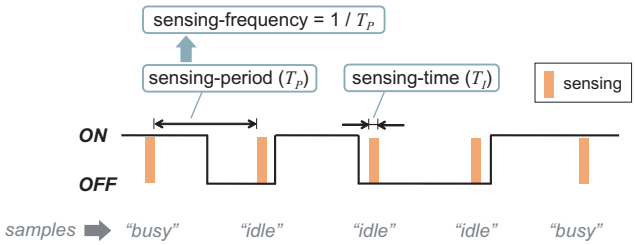

Figure 2: The ON/OFF channel model and periodic sensing process with sensing-period T_P and sensing-time T_I

local decision maker. Sun *et al.* [14] enhanced performance by clustering sensors where the benefit comes from cluster and sensor diversities. None of these authors, however, mentioned the importance of optimizing cluster size and sensor density.

Despite extensive existing studies on the performance of one-time signal detection in CRs, the optimal scheduling of in-band sensing has been received far less attention. Cordeiro *et al.* [6] evaluated the performance of fast sensing in 802.22 by scheduling fast sensing (1 ms) every 40 ms, but they did not optimize the sensing-time and sensing-period (or equivalently, sensing-frequency). Datla *et al.* [24] proposed a backoff-based sensing scheduling algorithm, but their scheme was not designed for detecting returning PUs in an in-band channel. Hoang and Liang [25] introduced an adaptive sensing scheduling method to capture the tradeoff between SUs' data-transmission and spectrum-sensing. Their scheme, however, did not focus on in-band sensing for protection of PUs.

1.4 Organization

Section 2 briefly reviews IEEE 802.22, followed by a summary of spectrum sensing including fine/fast sensing details. In Section 3, we first introduce the concept of sensor clustering, and then derive the maximum radius of a cluster as well as the maximum sensor density. Section 4 describes the proposed in-band sensing algorithm that can be used in a cluster. We consider two factors in building the algorithm: (1) noise uncertainty and (2) existence of interfering secondary networks (SNs). The performance of the proposed in-band sensing algorithms is evaluated in Section 5, and the paper concludes in Section 6.

2. PRELIMINARIES

2.1 IEEE 802.22

In this paper, we consider the scheduling of in-band sensing in an IEEE 802.22 network. Note, however, that our proposed schemes can be applied to future CR standards with no/slight modifications.

The IEEE 802.22 network is an infrastructure-based wireless network where a Base Station (BS) coordinates nodes in a single-hop cell which covers an area of radius ranging from 33 km (typical) to 100 km. End-users of an 802.22 cell are called *Consumer Premise Equipments* (CPEs) representing households in a rural area (and hence stationary nodes).

802.22 reuses UHF/VHF bands where three types of primary signals present: Analog TV, Digital TV, and wireless microphones. Our proposed schemes in this paper consider DTV transmitters as the major source of primary transmission; their extension for wireless microphones is part of our future work. By considering the minimum D/U (Desired to Undesired) signal ratio of 23 dB and the DTV protection contour of 134.2 km, the keep-out radius of CPEs from the DTV transmitter is given as 150.3 km [19]. CPEs within this keep-out radius are forced to avoid use of the DTV channel. Fig. 1 illustrates this scenario.

2.2 Channel and Sensing Model

A channel is modeled as an ON/OFF source, where an ON period represents the time duration during which PUs are actively using their channel. SUs are allowed to utilize the channel only during PUs' OFF periods. This model has been used successfully in modeling the PUs' channel-usage pattern in many applications [26–28]. A TV transmitter's channel usage pattern usually has very long (in the order of hours) ON and OFF periods.

Spectrum sensing is akin to sampling in that it measures a channel's state during the *sensing time* (denoted as T_I) and detects the presence of PU signals at that moment. T_I may vary with detection methods (e.g., less than 1 ms for energy detection). Fig. 2 illustrates the ON/OFF channel model and an example periodic sensing process with sensing-time T_I and sensing-period T_P.

In 802.22, sensing must be performed during a quiet period within which no CPEs are allowed to transmit data so that any signal activity detected by sensors should originate from the PUs. The quiet periods have to be synchronized among sensors in the same cell as well as between neighboring cells, which is achieved by the Coexistence Beacon Protocol (CBP) via exchange of CBP frames [6].

2.3 Signal Detection Methods

We briefly overview the detection methods used in IEEE 802.22, along with their theoretical performance in terms of P_{MD} and P_{FA}.

2.3.1 *Energy Detection*

Energy detection is the most popular for signal detection due to its simple design and small sensing time. Shellhammer *et al.* [19] analyzed the energy detection of a DTV signal using its discrete-time samples, where the signal is sampled by its Nyquist rate of 6 MHz.[4] The detection threshold γ to

[4]The DTV signal ranges from -3 MHz to +3 MHz in the baseband.

yield P_{FA} is given as

$$\gamma = N_d B \left(1 + \frac{Q^{-1}(P_{FA})}{\sqrt{M}}\right), \quad (2)$$

and P_{MD} with γ is given as

$$P_{MD} = Q\left(\frac{\sqrt{M}}{P + N_d B}\left[(P + N_d B) - \gamma\right]\right). \quad (3)$$

where M is the number of samples, N_d the noise power spectral density (PSD), B the signal bandwidth (6 MHz), P the signal power, and $Q(\cdot)$ the Q function.

Note that the effect of multipath fading is insignificant in detecting a DTV signal due to frequency diversity over the 6 MHz band [18, 19]. Instead, the impact of shadow fading must be considered in the variation of RSS at different sensor locations. Ghasemi and Sousa [10] derived the average performance of energy detection by numerically integrating P_{MD} over the fading statistics.

2.3.2 *Feature Detection*

Feature detection captures a specific signature of a DTV signal, such as pilot, field sync, segment sync, or cyclostationarity [6]. Each feature detector is reviewed briefly for completeness.

ATSC uses 8-VSB to modulate a DTV signal, and an offset of 1.25 is added to the signal which creates a *pilot signal* at a specific frequency location. The authors of [21] introduced pilot energy detection which filters the DTV signal with a 10 KHz narrowband filter at the pilot's frequency location. They showed that the pilot signal's SNR is 17 dB higher than the DTV signal's SNR, making the pilot a strong feature to detect.

A DTV data segment starts with a *data segment sync* of pattern {+5 -5 -5 +5}. A data field consists of 313 data segments, and the first data segment of each data field is called a *field sync segment* which contains special pseudo-random sequences: PN511 and PN63. Therefore, segment sync and field sync can be used as a unique feature of DTV signal. Detectors of such features are introduced by many researchers, such as [6,13,29,30], but no analytical derivation of P_{MD} and P_{FA} has been reported, i.e., they were evaluated only via simulation.

Since the DTV signal is digitally modulated, it shows the cyclostationary feature. Recently, Goh *et al.* [23], Han *et al.* [31], and Chen *et al.* [13] studied cyclostationary detection of ATSC and DVB-T DTV signals and investigated its performance via simulation, since the derivation of P_{MD}/P_{FA} of cyclostationary detectors for complex modulation schemes (e.g., 8-VSB) are known to be mathematically intractable [32].

In this paper, we choose the pilot energy detector among feature detectors for an illustrative purpose and use it to evaluate the tradeoffs between energy and feature detection, since its performance has been mathematically analyzed in [21]. Other types of feature detection, however, can also be used for our proposed method in Section 4 by evaluating P_{MD} and P_{FA} via simulation at a detection threshold we are interested in, for which the real DTV signal capture data in [33] and the sensing simulation model in [34] can be utilized.

P_{MD} and P_{FA} of the pilot energy detector (will henceforth be called simply "pilot detector") are derived similarly to energy detection and well described in [21]. Shellhammer and Tandra [21] stated that the pilot signal's SNR may be degraded due to both uncertainty in the pilot locations over 59 KHz and inaccuracy in the local oscillator (LO) of the low pass filter, which forces the detector to use a 70 KHz bandpass filter. Therefore, we will use the sampling frequency of 70 KHz, instead of 10 KHz, in our analysis. Unlike energy detection in a 6 MHz bandwidth, Rayleigh fading becomes a significant factor, as it is flat in the narrow band of 70 KHz. Hence, we will consider both Rayleigh and lognormal shadow fading in deriving P_{MD} and P_{FA} of pilot detection.

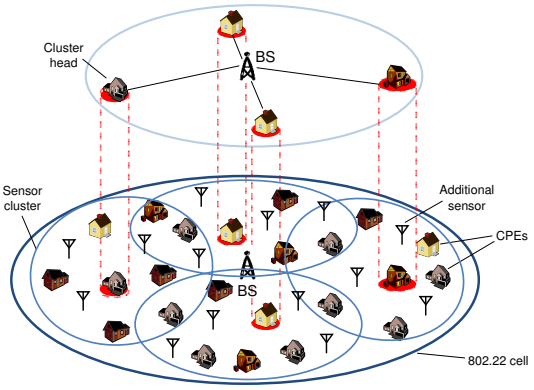

Figure 3: An illustration of clustered sensor networks in an IEEE 802.22 cell

3. SPECTRUM SENSOR CLUSTERING

As discussed in Section 1, the performance of collaborative sensing can be enhanced by clustering sensors in the network to make the gain of collaborative sensing more predictable. Sensor clustering can also make a sensor network scalable in collecting measurements for data fusion by enabling cluster heads (CHs) to make local decisions. The concept of a 2-tiered sensor cluster network is illustrated in Fig. 3.

We identify two important challenges in sensor clustering: cluster size and sensor density.

3.1 Cluster Size

We will derive the maximum radius of a sensor cluster so that the variation of average RSS within a cluster will be bounded by 1 dB, to make it possible to use Eq. (1) in modeling the performance of a collaborative sensor network. The effect of fading is considered by averaging P_{MD} of Eq. (3) over the fading statistics (Rayleigh fading or lognormal shadowing) and by substituting the result in Eq. (1).

According to the path-loss model of polynomial power decay [35], the average RSS at a sensor r meters away from a primary transmitter (PT) is given as $P_1 r^{-\alpha_{12}}$, where P_1 is the PT's transmit power and α_{12} is the path loss exponent. The maximum variation of the average RSS in a cluster is found between two sensors located at $(R - R_{cluster})$ and $(R + R_{cluster})$ meters away from the PT, respectively, where R is the distance between the PT and the center of a cluster, and $R_{cluster}$ is the radius of a cluster. Therefore, the maximum cluster size is determined as

$$10\alpha_{12} log_{10}\left(\frac{R + R_{cluster}}{R - R_{cluster}}\right) \leq 1(dB),$$

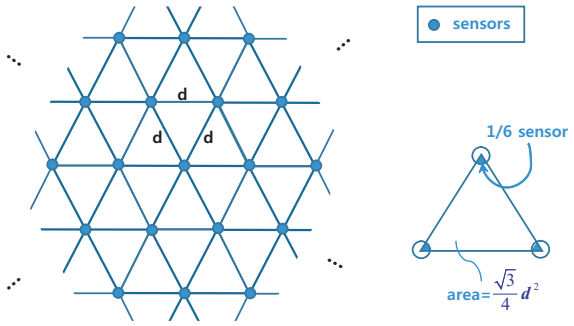

Figure 4: An example hexagonal deployment of spectrum sensors

which gives

$$R_{cluster} = \frac{\beta - 1}{\beta + 1} R, \quad \beta = 10^{0.1/\alpha_{12}}.$$

For example, for a cluster at the keep-out radius of 150.3 km (i.e., $R = 150.3$ km), $R_{cluster}$ is given as 5.76 km, using $\alpha_{12} = 3$ suggested in the Hata model [36–38].[5]

3.2 Sensor Density

Mishra *et al.* [16] claimed that a few tens of independent sensors provide as much collaborative gain as many more correlated sensors whose collaborative gain is limited by geographical correlation in shadowing. According to Gudmundson's model [17], the shadow correlation decays exponentially as distance between two locations increases. As a result, a blind increase in sensor density does not yield a linear increase of collaborative gain. Therefore, we will explore the maximum sensor density to guarantee enough distance between sensors for near-independent observations. We will also show that the minimum sensor density provides a sufficient number of minimally-correlated sensors in a cluster.

The shadow correlation between two locations that are d meters apart is given as $R(d) = e^{-ad}$, $a = 0.002$, in a suburban area [11, 17]. We want to suppress the correlation to be, on average, less than 0.3 between any two neighboring sensors. That is, $R(d) = e^{-0.002d} \leq 0.3$, which gives $d \geq 602$ m.

Assuming the hexagonal deployment of sensors as shown in Fig. 4, where the minimum distance between neighbors is d, the density of sensors (D_S) is shown to be

$$D_S = \frac{2}{\sqrt{3}d^2} (\text{sensors/m}^2),$$

and hence for $d = 602$ m, the maximum sensor density is

$$D_S^{max} = 3.18 (\text{sensors/km}^2).$$

The minimum sensor density (D_S^{min}) is determined by the household density, since a household represents a CPE which plays role as both a sensor and a transceiver. According to the WRAN reference model [40], the minimum household density in a rural area is 0.6 (houses/km^2). Therefore, the minimum sensor density is

$$D_S^{min} = 0.6 (\text{sensors/km}^2).$$

The next question is: at D_S^{min}, are there enough (i.e., at least 10 or more) sensors in a cluster for collaboration? Using the above-derived D_S^{min} and D_S^{max}, the number of sensors in a cluster ranges between N_{sensor}^{min} and N_{sensor}^{max} where

$$N_{sensor}^{min} = D_S^{min} \cdot \pi {R_{cluster}}^2,$$
$$N_{sensor}^{max} = D_S^{max} \cdot \pi {R_{cluster}}^2.$$

With $R_{cluster} = 5.76km$, this gives 62∼331 sensors per cluster which exceeds the recommendation in [16]. Therefore, the CH can select a subset of sensors for each quiet period in such a way that its area can be covered evenly.

Analog TV (NTSC)	-94 dBm (at peak of sync of the NTSC picture carrier)
Wireless Microphones	-107 dBm (200 KHz bandwidth)
Digital TV (ATSC)	-116 dBm (6 MHz bandwidth)

Table 1: Incumbent detection threshold (IDT) of primary signals

3.3 Discussion

In a real deployment scenario, the location of CPEs is not determined by the hexagonal model, since they are likely to be cluttered within small areas (e.g., a town or a village) where the actual sensor density is much higher than the average household density (e.g., 0.6 houses/km^2). On the other hand, CPEs are rare outside the populated areas. Therefore, we take two approaches: (1) the CHs in a populated area should selectively choose CPEs according to the recommended sensor density to avoid correlated measurements, and (2) the wireless service provider (WSP) has to deploy additional sensors in less-populated areas to achieve D_S^{min} (as shown in Fig. 3). In either case, the hexagonal model may be still useful in determining the proper locations of CPEs to be selected or sensors to be deployed.

A sensor cluster may be further divided into smaller subclusters to detect localized deep shadow fading which is not represented well by the lognormal shadowing model. In this case, sensors more than N_{sensor}^{max} can be elected in each cluster so that their *correlated* measurements can be used to identify any localized shadowing. Further development of sub-clustering may be possible, but it is left as our future work.

4. SCHEDULING OF IN-BAND SENSING

4.1 Sensing Requirements in IEEE 802.22

We briefly overview the sensing requirements in IEEE 802.22. *Incumbent detection threshold* (IDT) is the weakest primary signal power (in dBm) above which sensors should be able to detect. IDTs for three types of primary signals (in the US) [7] are shown in Table 1. As mentioned earlier, we will focus on DTV signals.

Channel detection time (CDT) is given to be ≤2 seconds, within which the returning PUs must be detected with

[5]Although the Hata model is not the best fit for 802.22 since it is designed to describe power decay of the transmitted signal up to 20 km from the PT, it works better than the widely-accepted Okumura model [39] which does not deal with rural environments. In this paper, we consider α_{12} as a design parameter and evaluate our schemes with $\alpha_{12} = 3$ as an example. Determination of α_{12} is outside of the scope of this paper.

$P_{MD} \leq 0.1$, regardless of the number of times sensing is performed during CDT. Similarly, $P_{FA} \leq 0.1$ must also be met when the same sensing algorithm used to meet $P_{MD} \leq 0.1$ is run for CDT seconds during which no PUs are present. The requirement on P_{MD} is to guarantee minimal interference to incumbents, whereas the requirement on P_{FA} is to avoid unnecessary channel switching due to false detection of PUs.

Based on the above interpretation of P_{MD} and P_{FA}, the two performance metrics can be expressed as

$$\begin{aligned} P_{MD} &= \Pr(\text{detect PT within } CDT \mid H_1) \leq 0.1, \\ P_{FA} &= \Pr(\text{detect PT within } CDT \mid H_0) \leq 0.1, \end{aligned} \quad (4)$$

where H_0 and H_1 are two hypotheses on the presence of PUs in the channel:

$$\begin{aligned} H_0: &\quad \text{No PU exists in the channel,} \\ H_1: &\quad \text{PUs exist in the channel.} \end{aligned}$$

Note that P_{MD} and P_{FA} in Eq. (4) have different meanings from those in Eq. (1). P_{MD} and P_{FA} in Eq. (4) are the probabilities measured by monitoring an in-band channel for CDT seconds during which sensing may be scheduled *multiple times*, whereas P_{MD} and P_{FA} in Eq. (1) are the probabilities of *one-time* sensing. To avoid any confusion, we will henceforth replace P_{MD} and P_{FA} in Eq. (4) with P_{MD}^{CDT} and P_{FA}^{CDT}.

4.2 TSS mechanism in IEEE 802.22

To support a sensing algorithm to meet the detectability requirements shown in Eq. (4), IEEE 802.22 provides the two-stage sensing (TSS) mechanism. With TSS, a sensing algorithm schedules either *fast* or *fine* sensing in each quiet period (QP), where fast sensing employs energy detection while fine sensing uses feature detection.

Although a sensing algorithm can schedule as many QPs as it wants, there are some restrictions on the sensing period. For example, the QP of fast sensing, usually less than 1 ms, should be scheduled at the end of an 802.22 MAC frame (10 ms) at most once in each frame. Hence, the period of fast sensing becomes a multiple of the frame size (i.e., $n \cdot 10$ ms, n: positive integer). On the other hand, the QP duration of fine sensing varies with the feature detection scheme used. In case the feature-detection scheme requires the sensing-time longer than one MAC frame (e.g., 24.2 ms for DTV field sync detection), its QP should be scheduled over consecutive MAC frames.

4.3 In-band Sensing Scheduling Algorithm

An efficient sensing algorithm must capture the tradeoff between fast and fine sensing: for one-time sensing, (1) fast sensing consumes a minimum amount of time but its performance is more susceptible to noise uncertainty and co-channel interference, and (2) fine sensing usually requires much more time than fast sensing, but its performance is better than fast sensing. Therefore, the sensing algorithm may have to schedule fast sensing at a high frequency, or it may decide to schedule fine sensing at a lower frequency. In either case, the scheduling goal is to minimize the overall time spent for sensing (or the *sensing-overhead*) while meeting the detectability requirements.

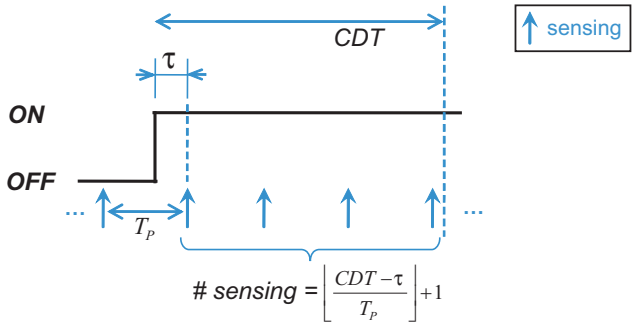

Figure 5: An example of periodic sensing when a channel transits from OFF to ON due to returning PUs.

4.3.1 Analysis of In-band Sensing Scheduling

We consider periodic fast or fine sensing. Suppose both fast and fine sensing consume less than 10 ms (i.e., one MAC frame size) for one-time sensing. Then, the sensing-period T_P is given as

$$T_P = n \cdot FS, \;\; 1 \leq n \leq \left\lfloor \frac{CDT}{FS} \right\rfloor, \;\; n \in \mathbb{N},$$

where FS is the MAC frame size. The upper-bound of T_P is necessary since sensing must be performed at least once every CDT seconds.

When the channel state changes from OFF to ON due to returning PUs as shown in Fig. 5, periodic sensing will measure the channel M times in CDT seconds, where

$$M = \left\lfloor \frac{CDT - \tau}{T_P} \right\rfloor + 1.$$

Each (one-time) sensing in Fig. 5 represents collaborative sensing with N sensors whose performance is described by Eq. (1). The value of N lies between N_{sensor}^{min} and N_{sensor}^{max} which were derived in Section 3.

We assume that τ/T_P is uniformly distributed in $[0, 1]$ since ON/OFF periods (in the order of hours) are in general much larger than T_P (less than 2 seconds). Under this assumption, the probability mass function (pmf) of M is derived as:

$$\begin{aligned} p(M_1) &= \Pr\left(M = \left\lfloor \frac{CDT}{T_P} \right\rfloor\right) = 1 - \frac{CDT}{T_P} + \left\lfloor \frac{CDT}{T_P} \right\rfloor, \\ p(M_2) &= \Pr\left(M = \left\lfloor \frac{CDT}{T_P} \right\rfloor + 1\right) = \frac{CDT}{T_P} - \left\lfloor \frac{CDT}{T_P} \right\rfloor. \end{aligned}$$

Then, P_{MD}^{CDT} can be expressed as:

$$\begin{aligned} P_{MD}^{CDT} &= \sum_M \Pr(\text{all } M \text{ sensings fail to detect the PU} | H_1) p(M) \\ &= \sum_M \left(P_{MD}(N)\right)^M p(M) \\ &= \sum_M \left(P_{MD}\right)^{NM} p(M) \;\; \leq 0.1. \end{aligned} \quad (5)$$

Similarly, P_{FA}^{CDT} can be expressed as:

$$\begin{aligned} P_{FA}^{CDT} &= 1 - \sum_{M} \Pr(\textit{none of } M \text{ sensings detects PUs} | H_0) p(M) \\ &= 1 - \sum_{M} \left(1 - P_{FA}(N)\right)^{M} p(M) \\ &= 1 - \sum_{M} \left(1 - P_{FA}\right)^{NM} p(M) \quad \leq 0.1. \end{aligned} \tag{6}$$

In Eqs. (5) and (6), P_{MD} and P_{FA} are detection-method specific. They also depend on the sensing-time (T_I) and the RSS of the primary signal. P_{MD} and P_{FA} of energy and pilot detectors are fully described by Eqs. (2) and (3).

4.3.2 The Proposed Sensing Scheduling Algorithm

Our objective is to find the optimal sensing-period T_P for given T_I and RSS, that minimizes the sensing overhead while satisfying two conditions of Eqs. (5) and (6). The sensing-overhead of a sensing algorithm is defined as the fraction of time in which sensing is performed. That is,

$$\text{sensing-overhead} = \frac{T_I}{T_P}$$

for periodic sensing.

The problem of optimizing T_P is identical to that of maximizing n that satisfies Eqs. (5) and (6). Therefore, the proposed algorithm examines n from its upper bound $\lfloor CDT/FS \rfloor$ and decreases n until the one that meets the condition is found.

Since P_{FA}^{CDT} is a monotonic function[6] of P_{FA} and there is a one-to-one mapping between P_{FA} and P_{MD}, we first want to find the value of P_{FA} that solves the equality of Eq. (6). Then, P_{MD} corresponding to P_{FA} can be found from the ROC curve between them. Finally, the feasibility of the tested n can be checked by substituting P_{MD} into Eq. (5). If the tested n does not satisfy Eq. (5), then n is decreased by 1 and the above procedure is repeated.

If there does not exist any n satisfying both equations, the detection method considered cannot meet the detectability requirements with given T_I and RSS. On the contrary, if the optimal sensing period is found at $n = n_{opt}$, its sensing overhead is determined as: $T_I/(n_{opt} \cdot FS)$.

The pseudo-code of the proposed algorithm for energy and pilot detection is given in Fig. 6.

4.3.3 Implementation Issues

An important aspect of the proposed algorithm is that it computes the optimal sensing periods offline, and the optimal periods can be looked up from the database with two inputs, T_I and RSS, at runtime. A sensor can create/store one database per detection method, and adaptively choose the best method with optimal T_P and T_I.

Note that P_{MD} and P_{FA} of a single sensor to meet Eqs. (5) and (6) are functions of N. This suggests that IEEE 802.22 may need to refine its definition/requirement on P_{MD} and P_{FA} so that they can be determined adaptively taking N as a variable.

In Section 5, we will evaluate and compare the performance of energy and pilot detection. The optimal sensing strategy (i.e., optimal detection, period, and time) with the average RSS varying from -120 dBm to -90 dBm will also be proposed.

[6]One can easily show this by differentiating P_{FA}^{CDT} with respect to P_{FA}.

```
n := ⌊CDT/FS⌋;

while (n > 0) {
    P_FA := {x|1 − Σ_M (1 − x)^NM p(M) = 0.1};
    γ := N_d B(1 + Q^−1(P_FA)/√M);
    P_MD := Q([(P + N_d B) − γ] · √M/(P + N_d B));
    if (P_MD^CDT(P_MD) ≤ 0.1)   then {
      ⟨set sensing-period: T_P = n · FS⟩;
      return;
    }
    else   n := n − 1;
}
⟨mark the current detection method infeasible⟩;
return;
```

Figure 6: Pseudo-code of the in-band sensing scheduling algorithm

5. PERFORMANCE EVALUATION

5.1 Two Important Factors in In-band Sensing

5.1.1 Noise Uncertainty

Below a certain SNR threshold, called SNR_{wall} [1], energy detection in the AWGN channel is found to completely fail to detect a signal irrespective of the amount of sensing-time used. SNR_{wall} results from the uncertainty in the noise power (called *noise uncertainty*), and their relationship is given as

$$SNR_{wall} = \frac{\rho^2 - 1}{\rho},$$

when $\rho = 10^{x/10}$ and x is the noise uncertainty in dB. In [41], the amount of noise uncertainty is shown to depend on four factors: calibration error, thermal variation, changes in low-noise amplifier (LNA) gain, and interference, where the noise uncertainty under 20 °K of temperature variation is given as ± 1 dB.

Based on this finding, energy detection is often considered unsuitable for CRNs which must detect very weak signal power (e.g., as low as -116 dBm for DTV signals). However, we found that SNR_{wall} can actually be overcome even when the average SNR (by the aRSS) is less than SNR_{wall}, via the location diversity of collaborative sensing. Although SNR_{wall} plays role as an absolute barrier when the AWGN channel is considered, the energy detection of DTV signals will experience a lognormal shadow-fading channel with which SNR_{wall} becomes penetrable because at some sensor locations instantaneous SNR may exceed SNR_{wall} even if the average SNR in the sensor network is below the wall.

The effect of shadow-fading can be clearly observed in Figs. 7 and 8, where dB-spread of 5.5 dB [34] is used for shadow-fading. In general, the performance under shadow-fading channel is worse than the AWGN channel. However, from Fig. 7, one can see that the performance of a shadow-fading channel becomes even better than the AWGN channel at a low SNR (the smaller P_{MD}, the better the performance).

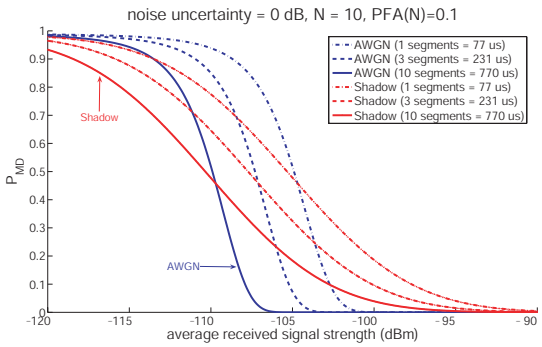

Figure 7: Performance comparison (in P_{MD}) of energy detection: AWGN channel vs. shadow-fading channel (when noise uncertainty is 0 dB).

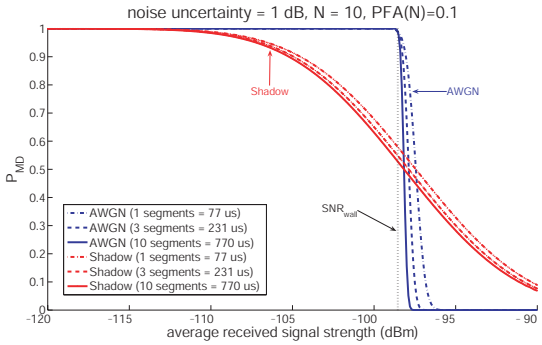

Figure 8: Performance comparison (in P_{MD}) of energy detection: AWGN channel vs. shadow-fading channel (when noise uncertainty is 1 dB).

When there exists noise uncertainty of 1 dB as in Fig. 8, this effect becomes more pronounced.[7] As predicted in [1], no energy detector among N sensors under the AWGN channel overcomes SNR_{wall} of -3.33 dB (illustrated as a horizontal dotted line at $RSS = -98.5$ dBm in the figure). Under the shadow-fading channel, however, some sensors under constructive shadow-fading[8] may have SNR greater than SNR_{wall} which contributes to the performance enhancement over the AWGN channel. Note that other sensors under destructive shadow-fading does not degrade the overall performance, since their instantaneous RSSs are already below SNR_{wall}, where P_{MD} is always equal to 1.

On the other hand, SNR_{wall} of feature detection decays as the channel coherence time increases [18], meaning that SNR_{wall} in feature detection is insignificant, since 802.22 CPEs and BSs are stationary devices.

In this section, various noise uncertainties of 0, 0.5, 1, 2 dB will be tested and their effects on each detection method will be investigated.

[7]We followed the worst-case analysis in [20] where the upper (lower) limit of noise PSD is used to calculate P_{FA} (P_{MD}), when noise uncertainty is Δ dB and the range of noise PSD is given as $-163 \pm \Delta$ (dBm/Hz).

[8]Constructive fading happens under lognormal shadowing, because the instantaneous RSS (in dB) is modeled as "average RSS (dB) + X (dB)" where X is a zero-mean Gaussian random variable.

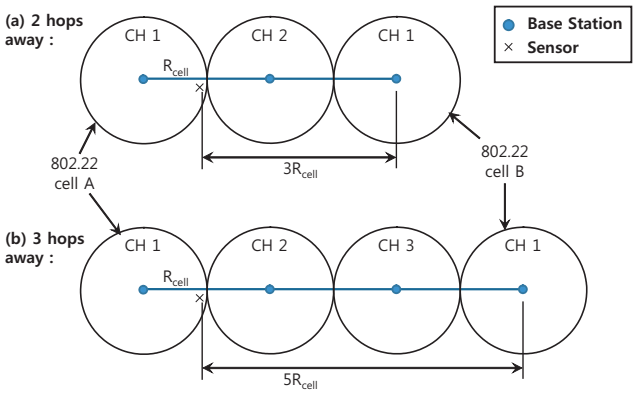

Figure 9: Inter-cell interference scenarios in 802.22

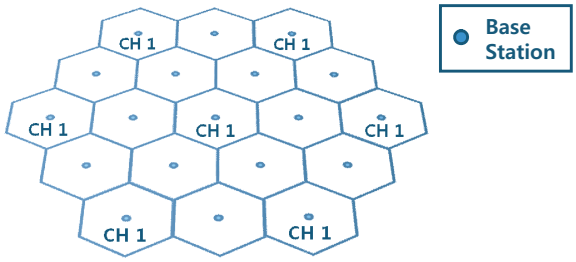

Figure 10: The worst-case channel assignment to have maximal inter-cell interference

5.1.2 *Inter-CRN Co-channel Interference*

Although the perfect synchronization of QPs between neighboring 802.22 cells is guaranteed by the CBP protocol, 802.22 cells more than one-hop away may be assigned the same channel. In such a case, they could introduce non-negligible interference to the CPEs. Moreover, future CRN standards other than IEEE 802.22 may co-exist in the same TV bands, which will cause additional interference to 802.22 cells. We call this type of interference *inter-CRN co-channel interference*.

We first evaluate how much interference is expected between 802.22 cells that are m hops apart from each other. Fig. 9 shows two scenarios of co-channel interference. In (a), cell A's two-hop neighbor cell B uses the same channel 1, which will interfere with the sensor at the border of cell A. According to [40], a BS with coverage radius of 35 km will have transmit EIRP of 23.5 dBW, when its antenna has a typical height of 75 m [42]. The interference power of cell B's BS[9] to the sensor is then given as

$$\begin{aligned} P_{\text{cell B's BS}} \cdot (3R_{cell})^{-\alpha} &= 10^{23.5} \cdot (3 \cdot 33 \times 10^3)^{-3} \ W \\ &= -96.5 \ dBm, \end{aligned}$$

which is comparable to the noise power of -95.2 dBm in the 6 MHz band [19]. On the other hand, in (b), two cells that are three hops apart result in the interference power of -103 dBm, which is negligible. Hence, we only consider interference from two-hop neighbors.

Fig. 10 shows the worst-case scenario of channel assign-

[9]Note that the CPEs in cell B are not significant interferers as a CPE uses a directional antenna to communicate with its BS which minimizes its emitted power to the outside of its cell.

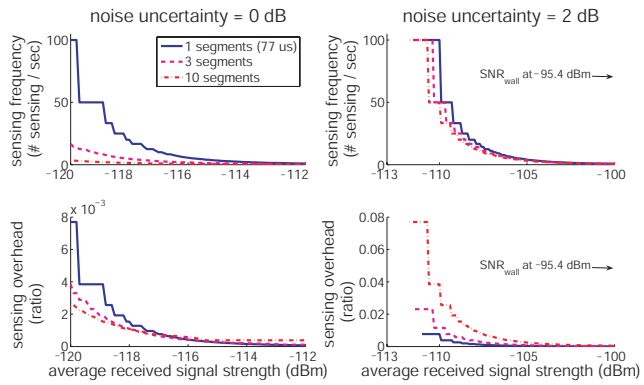

Figure 11: Energy detection: sensing-overhead and sensing-frequency (left-half: noise uncertainty = 0 dB; right-half: noise uncertainty = 2 dB)

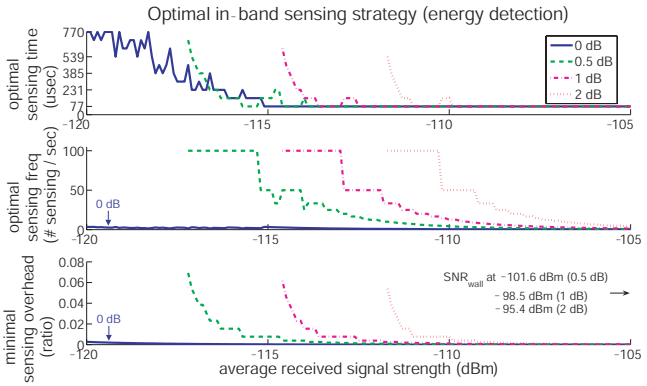

Figure 12: Energy detection (varying noise uncertainty): optimal sensing-time/frequency, and minimal sensing-overhead

ment for the central 802.22 cell to have maximal inter-CRN interference. There can be up to 6 two-hop interfering neighbors of a cell. Thus, the interference power will vary from $-\infty$ dBm (i.e., no interference) to -88.7 dBm (6 times larger than -96.5 dBm) in our numerical analyses.

5.2 Optimal Sensing-time and Sensing-frequency

We evaluate energy and pilot detection to find the optimal sensing-time (T_I) and sensing-frequency ($1/T_P$) to minimize the sensing overhead, when they meet the detectability requirements of $P_{MD}^{CDT}, P_{FA}^{CDT} \leq 0.1$.

Each detection scheme is evaluated while varying the average RSS (of the 6 MHz DTV signal) from -120 dBm to -90 dBm in step of 0.1 dBm. This RSS range is chosen because (1) the IDT of DTV signal is -116 dBm, and (2) RSS at the keep-out radius of a DTV transmitter is -96.48 dBm [19]. Therefore, our interest lies in the range between -116 dBm and -96.48 dBm, which is well covered by the simulated RSS range.

We study the impact of noise uncertainty by varying the uncertainty to 0 dB, 0.5 dB, 1 dB, or 2 dB, with the number of cooperative sensors fixed at $N = 10$. The effect of inter-CRN interference is also evaluated by changing the number of interfering 802.22 cells (two-hop neighbors) to 1, 2, 4, or 6 cells, with $N = 20$ and the noise uncertainty = 1 dB.

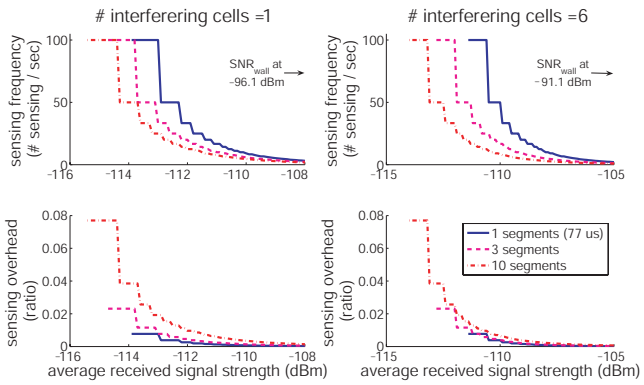

Figure 13: Energy detection: sensing-overhead and sensing-frequency (left-half: 1 interfering cell; right-half: 6 interfering cells)

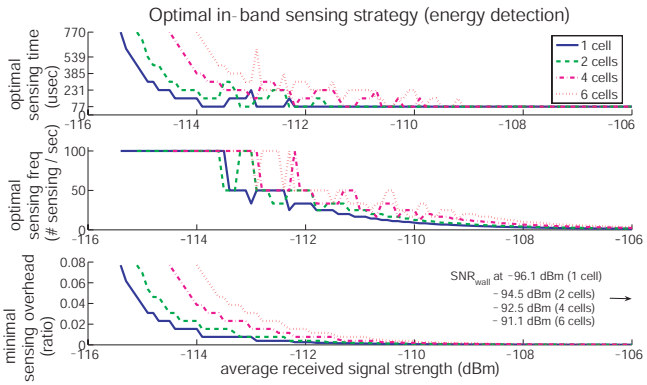

Figure 14: Energy detection (varying inter-CRN interference): optimal sensing-time/frequency, and minimal sensing-overhead

5.2.1 *Energy Detection*

Since one data segment of a DTV signal is 77 μs, we tested 10 different sensing-times for energy detection, such as $k \cdot (77\mu s)$, $k = 1, 2, \ldots, 10$. During each sensing-time, the proposed sensing scheduling algorithm searches for the optimal sensing-frequency and the minimal sensing-overhead at every RSS value. After optimizing the sensing-frequency, the sensing overheads from 10 different sensing-times are compared and the best sensing-time at each RSS input is chosen.

First, we show the effects of noise uncertainty. Fig. 11 compares energy detection under no noise uncertainty (0 dB) with that of 2 dB noise uncertainty. For an illustrative purpose, three sensing-times (1, 3, 10 segments) are presented. For the 0 dB case, energy detection is shown to perform very well at any RSS with a negligible overhead (less than 0.3%). By contrast, with 2 dB noise uncertainty, energy detection becomes infeasible for RSS < -111.7 dBm. Note that the blank between -113 dBm and -111.7 dBm implies that there is no T_P satisfying the detectability requirements. However, compared to the AWGN's SNR_{wall} of -95.4 dBm, energy detection's feasibility region is enlarged significantly thanks to the sensor diversity under the shadow-fading channel. Another notable phenomenon is that performance (in terms of sensing overhead) does not get better as the sensing-

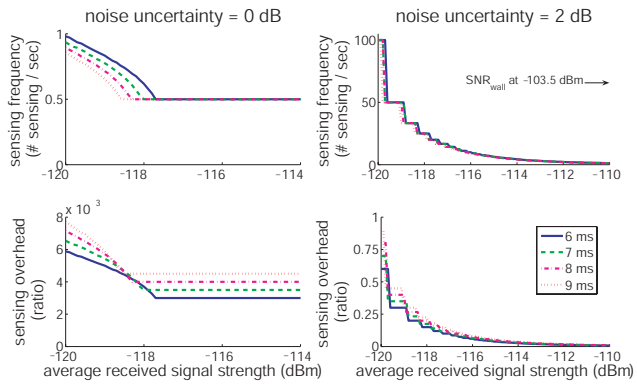

Figure 15: Pilot detection: sensing-overhead and sensing-frequency (left-half: noise uncertainty = 0 dB; right-half: noise uncertainty = 2 dB

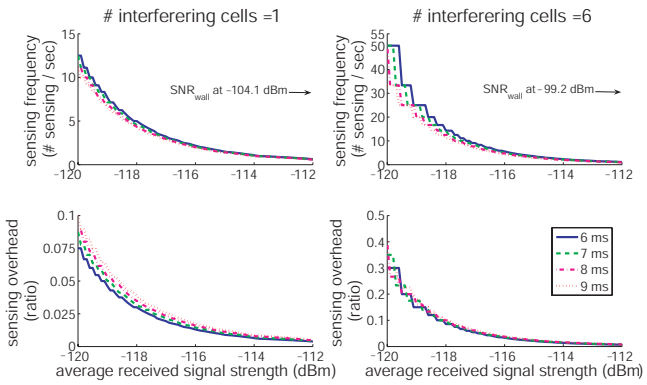

Figure 17: Pilot detection: sensing-overhead and sensing-frequency (left-half: 1 interfering cell; right-half: 6 interfering cells)

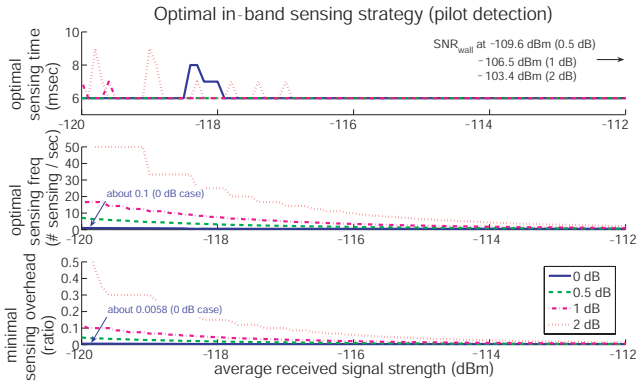

Figure 16: Pilot detection (varying noise uncertainty): optimal sensing-time/frequency, and minimal sensing-overhead

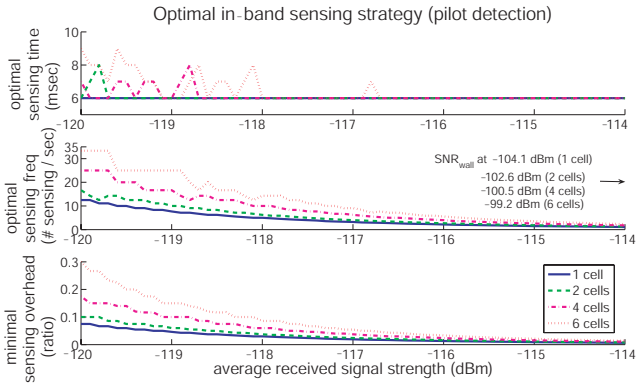

Figure 18: Pilot detection (varying inter-CRN interference): optimal sensing-time/frequency, and minimal sensing-overhead

time grows at 2 dB noise uncertainty, since the impact of SNR_{wall} becomes more dominant as the noise uncertainty increases. Fig. 12 shows the proposed in-band sensing strategy with the optimal sensing-time and frequency, along with the achieved minimal sensing overhead. As the average RSS gets smaller, both sensing-time and sensing-frequency must be increased to make energy detection feasible.

Second, we vary the number of interfering 802.22 cells to observe the behavior of energy detection. Fig. 13 shows two extreme cases: 1 cell vs. 6 cells. As expected, an increase of interfering cells increases the noise plus interference power which impairs performance due to degraded SNR. However, as can be seen in Fig. 14, the feasibility region is reduced just by 1.4 dB between 1 cell and 6 cells, whereas the gap is 5.5 dB in Fig. 12 between 0.5 dB and 2 dB noise uncertainties. Therefore, noise uncertainty seems to have a more significant influence on energy-detection's performance.

5.2.2 *Feature (Pilot) Detection*

Since pilot (energy) detection is based on the energy measurement of a pilot signal, it requires a sufficient number of samples to yield satisfactory results. Due to its lower sampling frequency, the sensing-time of pilot detection should be 85 times longer (6MHz/70KHz=85.7) than that of energy detection to acquire the same number of samples as energy detection. On the other hand, the MAC frame size of 10 ms gives an upper-bound of sensing-time. Based on this observation, we vary the sensing-time of pilot detection to be 6, 7, 8, or 9 ms, considering that $85.7 \times 77\mu s = 6.6$ ms.

Figs. 15 and 16 plot the performance of pilot detection while varying the noise uncertainty. Note that the x-axis represents the average RSS of a 6 MHz DTV signal, not of a pilot signal in the 70 KHz band. The power of pilot signal is 11.3 dB less than the DTV signal power. Unlike energy detection, pilot detection is feasible at every RSS regardless of the level of noise uncertainty, due to its higher SNR at the pilot location. 6 ms appears to be the optimal sensing-time for most cases, suggesting that the number of samples (M) is the limiting factor of pilot detection.

Figs. 17 and 18 show the performance of pilot detection while varying the number of interferers. At a given number of interfering cells, the sensing-time does not appear to offer a large performance enhancement. Similarly to Figs. 15 and 16, the sensing-time of 6 ms performs best except for the case of a very low SNR (i.e., RSS less than -118 dBm).

5.3 Energy Detection or Feature Detection?

Finally, we investigate the location of $aRSS_{threshold}$, below which pilot detection is preferred to energy detection. We also introduce $aRSS_{min}^{energy}$, the minimum aRSS above

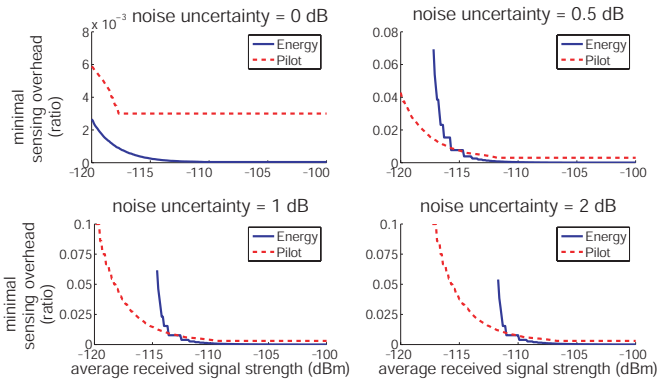

Figure 19: Energy detection vs. pilot detection: location of $aRSS_{threshold}$ (while varying the noise uncertainty)

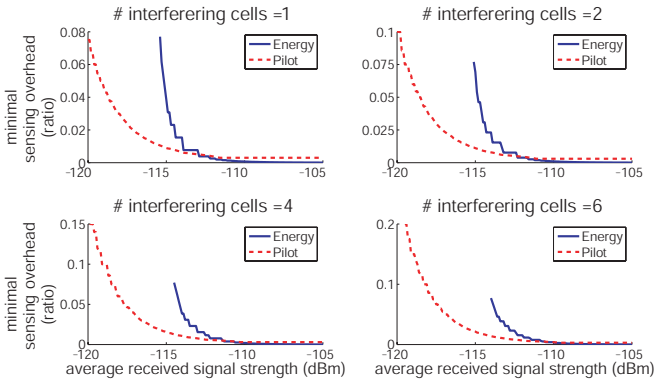

Figure 20: Energy detection vs. pilot detection: location of $aRSS_{threshold}$ (while varying the inter-CRN interference)

noise uncertainty	0.5 dB	1 dB	2 dB
$aRSS_{threshold}$ (dBm)	-114.6	-112.5	-109.9
$aRSS_{min}^{energy}$ (dBm)	-117.2	-114.6	-111.7

Table 2: $aRSS_{threshold}$ and $aRSS_{min}^{energy}$ with various noise uncertainty levels

# of interferers	1	2	4	6
$aRSS_{threshold}$ (dBm)	-112.9	-112.3	-111.3	-110.5
$aRSS_{min}^{energy}$ (dBm)	-115.4	-115.1	-114.5	-114

Table 3: $aRSS_{threshold}$ and $aRSS_{min}^{energy}$ with various inter-CRN interference levels

which energy detection becomes feasible for detection of DTV signals.

Fig. 19 compares the minimal sensing-overheads of energy and pilot detection under various noise uncertainty conditions. When there is no noise uncertainty, energy detection is the best to use. As the noise uncertainty grows, however, pilot detection becomes preferable at a low aRSS and $aRSS_{threshold}$ increases accordingly. The position of $aRSS_{threshold}$ is shown in Table 2 along with $aRSS_{min}^{energy}$. With 1 or 2 dB noise uncertainty, pilot detection is found to be feasible and preferable even at -120 dBm, but it incurs more than 10% of sensing overhead.

$aRSS_{threshold}$ and $aRSS_{min}^{energy}$ of various inter-CRN interference are also presented in Fig. 20 and Table 3. With 1 or 2 dB noise uncertainty, pilot detection is found to incur more than 15% of sensing overhead at -120 dBm.

5.4 Other Feature Detectors

From Figs. 19 and 20, one can observe that energy detection, above $aRSS_{threshold}$, incurs *at most* 0.385% of sensing overhead. Here, we compare this overhead with three other types of feature detectors than pilot-energy detection: the pilot-location detection in [43], the PN511 detection in [6], and the cyclostationary detection in [22]. Since sensing-times for such feature detectors are 30 ms, 24.1 ms, and 19.03 ms, respectively, their sensing overheads are given as *at least* 1.5, 1.2, and 0.95 % even when sensing is scheduled only once every CDT seconds. Therefore, energy detection performs better in its preferred region (i.e., above $aRSS_{threshold}$) than the pilot-energy as well as other three types of feature detectors under consideration.

6. CONCLUSION

In this paper, we proposed an optimal in-band sensing scheduling algorithm which optimizes the sensing-time and sensing-frequency of energy and feature detection, while meeting the sensing requirements in IEEE 802.22. Its performance has been evaluated extensively with respect to two important factors: noise uncertainty and inter-CRN interference. It is shown that energy detection under the shadow-fading channel is still feasible and effective in meeting the detectability requirements via collaborative sensing, and sometimes preferred to feature detection even when the average RSS is much lower than the power wall determined by SNR_{wall}. The necessity of sensor clustering in CRNs is also elaborated, and two important problems, sensor cluster size and sensor density, have been addressed.

In future, we would like to explore other types of feature detection and evaluate their performance comparatively with energy detection. In-band sensing of wireless microphones should be another important subject of our future work.

Acknowledgments

The work reported in this paper was supported in part by the US National Science Foundation under grants CNS-0519498 and CNS-0721529 and by industry grants from Intel Corporation, Philips Research North America, and NEC Labs North America.

7. REFERENCES

[1] R. Tandra and A. Sahai. Fundamental limits on detection in low SNR under noise uncertainty. In *Proc. of the WirelessCom 2005*, pages 464–469, June 2005.

[2] FCC. Spectrum policy task force report. *ET Docket No. 02-135*, November 2002.

[3] FCC. Facilitating opportunities for flexible, efficient, and reliable spectrum use employing cognitive radio technologies. *ET Docket No. 03-108*, December 2003.

[4] FCC. Notice of proposed rule making and order. *ET Docket No. 03-322*, December 2003.

[5] S. Haykin. Cognitive radio: brain-empowered wireless communications. *IEEE J-SAC*, 23(2):201–220,

February 2005.

[6] C. Cordeiro, K. Challapali, and M. Ghosh. Cognitive PHY and MAC layers for dynamic spectrum access and sharing of TV bands. *ACM TAPAS*, Aug. 2006.

[7] IEEE 802.22 working group on wireless regional area networks. http://www.ieee802.org/22/.

[8] G. Ganesan and Y. Li. Cooperative spectrum sensing in cognitive radio networks. In *Proc. of the IEEE DySPAN 2005*, pages 137–143, November 2005.

[9] E. Visotsky, S. Kuffner, and R. Peterson. On collaborative detection of TV transmissions in support of dynamic spectrum sharing. In *Proc. of the IEEE DySPAN 2005*, pages 338–344, November 2005.

[10] A. Ghasemi and E.S. Sousa. Opportunistic spectrum access in fading channels through collaborative sensing. *Journal of Communications (JCM)*, 2(2):71–82, March 2007.

[11] A. Ghasemi and E. S. Sousa. Collaborative spectrum sensing for opportunistic access in fading environments. In *Proc. of the IEEE DySPAN 2005*, pages 131–136, November 2005.

[12] A. Goldsmith. *Wireless Communications*. Cambridge University Press, Cambridge, NY, 2005.

[13] T. Chen, H. Zhang, G.M. Maggio, and I. Chlamtac. CogMesh: A cluster-based cognitive radio network. In *Proc. of IEEE DySPAN*, pages 168–178, Apr. 2007.

[14] C. Sun, W. Zhang, and K.B. Letaief. Cluster-based cooperative spectrum sensing in cognitive radio systems. *IEEE ICC*, pages 2511–2515, June 2007.

[15] P. Pawelczak, C. Guo, R.V. Prasad, and R. Hekmat. Cluster-based spectrum sensing architecture for opportunistic spectrum access networks. *IRCTR-S-004-07 Report*, February 2007.

[16] S. M. Mishra, A. Sahai, and R. W. Brodersen. Cooperative sensing among cognitive radios. In *Proc. of the IEEE ICC 2006*, pages 1658–1663, June 2006.

[17] M. Gudmundson. Correlation model for shadow fading in mobile radio systems. *Electronic Letters*, 27(23):2145–2146, November 1991.

[18] R. Tandra and A. Sahai. SNR walls for feature detectors. In *Proc. of the IEEE DySPAN 2007*, pages 559–570, April 2007.

[19] S. Shellhammer, S. Shankar N., R. Tandra, and J. Tomcik. Performance of power detector sensors of DTV signals in IEEE 802.22 WRANs. In *Proc. of the ACM TAPAS 2006*, August 2006.

[20] S. Shellhammer and R. Tandra. Performance of the power detector with noise uncertainty. *IEEE 802.22-06/0134r0*, July 2006.

[21] S. Shellhammer and R. Tandra. An evaluation of DTV pilot power detection. *IEEE 802.22-06/0188r0*, July 2006.

[22] H.-S. Chen, W. Gao, and D.G. Daut. Spectrum sensing using cyclostationary properties and application to IEEE 802.22 WRAN. In *Proc. of IEEE GLOBECOM*, pages 3133–3138, November 2007.

[23] L.P. Goh, Z. Lei, and F. Chin. DVB detector for cognitive radio. In *Proc. of the IEEE ICC 2007*, pages 6460–6465, June 2007.

[24] D. Datla, R. Rajbanshi, A.M. Wyglinski, and G.J. Minden. Parametric adaptive spectrum sensing framework for dynamic spectrum access networks. In *Proc. of IEEE DySPAN*, pages 482–485, Apr. 2007.

[25] A.T. Hoang and Y.-C. Liang. Adaptive scheduling of spectrum sensing periods in cognitive radio networks. In *Proc. of the IEEE GLOBECOM 2007*, pages 3128–3132, November 2007.

[26] H. Kim and K. G. Shin. Efficient discovery of spectrum opportunities with MAC-layer sensing in cognitive radio networks. *IEEE Transactions on Mobile Computing (T-MC)*, 7(5):533–545, May 2008.

[27] A. Motamedi and A. Bahai. MAC protocol design for spectrum-agile wireless networks: Stochastic control approach. In *Proc. of the IEEE DySPAN 2007*, pages 448–451, April 2007.

[28] S. Geirhofer, L. Tong, and B. M. Sadler. Dynamic spectrum access in the time domain: Modeling and exploiting white space. *IEEE Communications Magazine*, 45(5):66–72, May 2007.

[29] S. Shellhammer. An ATSC detector using peak combining. *IEEE 802.22-06/0243r0*, November 2006.

[30] M. Muterspaugh, H. Liu, and W. Gao. Thomson proposal outline for WRAN. *IEEE 802.22-05/0096r1*, November 2005.

[31] N. Han, S. Shon, J.H. Chung, and J.M. Kim. Spectral correlation based signal detection method for spectrum sensing in IEEE 802.22 WRAN systems. In *Proc. of the ICACT 2006*, pages 1765–1770, February 2006.

[32] A. Sahai and D. Cabric. Cyclostationary feature detection. *Tutorial presented at the IEEE DySPAN 2005 (Part II)*, November 2005. http://www.eecs.berkeley.edu/ sahai/Presentations/DySPAN05_part2.ppt.

[33] V. Tawil. DTV signal captures. *IEEE 802.22-06/0038r0*, March 2006.

[34] S. Shellhammer, V. Tawil, G. Chouinard, M. Muterspaugh, and M. Ghosh. Spectrum sensing simulation model. *IEEE 802.22-06/0028r10*, September 2006.

[35] A. Sahai, R. Tandra, S.M. Mishra, and N. Hoven. Fundamental design tradeoffs in cognitive radio systems. In *the ACM TAPAS 2006*, August 2006.

[36] M. Hata. Empirical formula for propagation loss in land mobile radio services. *IEEE Transactions on Vehicular Technology*, VT-29(3):317–325, August 1980.

[37] E. Sofer. WRAN channel modeling. *IEEE 802.22-05/0055r0*, July 2005.

[38] D. Mazzarese and B. Ji. Updated MIMO proposal for IEEE 802.22 WRAN systems. *IEEE 802.22-06/0015r0*, January 2006.

[39] T.S. Rappaport. *Wireless Communications: Principles and Practices*. Prentice Hall PTR, Upper Saddle River, NJ, 2nd edition, 2002.

[40] G. Chouinard. WRAN reference model. *IEEE 802.22-04/0002r12*, September 2005.

[41] S. Shellhammer. Numerical spectrum sensing requirements. *IEEE 802.22-06/0088r0*, June 2006.

[42] W. Caldwell. Draft recommended practice. *IEEE 802.22-06/0242r04*, March 2007.

[43] C. Cordeiro, M. Ghosh, D. Cavalcanti, and K. Challapali. Spectrum sensing for dynamic spectrum access of TV bands. In *Proc. of CrownCom*, July 2007.